Journal of *Marine Science and Engineering*

MDPI

Article

Adverse Impacts of Chokepoint Transit Restrictions on Sustainable Maritime Transport: A Scenario-Based Emission Analysis in the Strait of Hormuz

Kadir Mersin [1], İrşad Bayırhan [2,*] and Orcan Çetinkaya [1]

[1] Department of Logistics Management, Istanbul Gelisim University, Istanbul 34310, Türkiye; kmersin@gelisim.edu.tr (K.M.); orcetinkaya@gelisim.edu.tr (O.Ç.)
[2] Institute of Marine Sciences and Management, Istanbul University, Istanbul 34134, Türkiye
* Correspondence: ibayirhan@istanbul.edu.tr

Abstract

The Strait of Hormuz is a transit point of vital importance to the global energy supply; however, the operational and environmental burdens caused by transit disruptions have not been sufficiently examined. This study uses a scenario-based methodology to quantify the additional fuel consumption and associated CO_2, SO_x, NO_x, and $PM_{2.5}$ emissions from waiting at anchor and low-speed maneuvering, particularly for energy-carrying vessels. It further provides a comparative examination of emission impacts at the vessel and fleet scales under crisis scenarios, dynamically characterizing the relationship between waiting time and emission increase. The analyses reveal that prolonged waiting and controlled transit substantially increase fuel consumption and, consequently, emissions. At a fleet scale of 28 vessels per week in the Strait of Hormuz, additional CO_2 emissions reach 1401.12 tons under a moderate crisis and 2711.68 tons under a severe crisis, amounting to more than 10,400 tons of additional CO_2 per month. Moreover, the local NO_x and $PM_{2.5}$ emitted by auxiliary engines idling at anchorage areas constitute a cumulative environmental risk to coastal air quality. Main-engine-related route deviation is most prominent at Suez, whereas a low-speed regime predominates at Malacca. These findings demonstrate that geopolitical friction at strategic straits entails not only energy-supply risks but also serious environmental harm. Consequently, chokepoint vulnerability assessments and energy security policies should holistically integrate vessel-level operational dynamics with maritime emission planning.

Keywords: Strait of Hormuz; maritime chokepoint; chokepoint disruption; energy transport; fuel consumption; CO_2 emissions; LNG carriers; oil tankers; bottom-up emission modeling

Check for updates

Academic Editors: Jiaguo Liu and Bingmei Gu

Received: 27 August 2026
Revised: 15 September 2026
Accepted: 18 September 2026
Published: 20 September 2026

Copyright: © 2026 by the authors. Licensee MDPI, Basel, Switzerland. This article is an open access article distributed under the terms and conditions of the Creative Commons Attribution (CC BY) license.

1. Introduction

Transit restrictions in critical chokepoints are the most important risk factor that directly threatens global trade and supply chains. These restrictions in the Strait of Hormuz decrease the daily number of ships from 130 to single digits [1]. This situation creates pressure on maritime management and multimodal transport connections. However, all of these operational disruptions and bottlenecks in the strategic chokepoints lead to a significant increase in emission loads.

Attempted transit restrictions in the Strait of Hormuz also carry indirect risks for these chokepoints. For example, ships hide their flags, and ghost fleets are created by

these restrictions [2]. Furthermore, marine organisms accumulate on ships' hulls due to prolonged waiting times. These organisms are carried by ships and cause ecological damage risks [3]. Especially, the Strait of Malacca, which is the most important waterway between Asia and the Middle East/Europe, bears a lack of alternatives that would disrupt the raw material and energy supplies across all of East Asia in case of a restriction scenario, as the Strait of Hormuz does. Due to military restrictions and attacks on ships in the Bab-el-Mandeb Strait and the Red Sea, merchant ships divert their routes to the Cape of Good Hope instead of the Suez Canal [1,4]. Moreover, drought leads to periodic restrictions in the Panama Canal, escalating global freight rates as war risk premiums are seen in the Strait of Hormuz [2,4].

Nevertheless, beyond these macroeconomic and logistics effects, as of August 2026, energy consumption and environmental effects of more than 1500 merchant ships [5] that were held idle in the Persian Gulf for months due to bottlenecks in the Strait of Hormuz have not been sufficiently addressed. So, the main subject that has to be studied is ship-sourced emissions at the gate. These vessels cause both a sharp increase in greenhouse gas (GHG) emissions and severe local air pollution in port regions. Even if a merchant ship shuts down the main engine, auxiliary engines keep working to produce energy for electricity, cooling, heating, and living quarters. Thereby, fuel consumption never gets interrupted. Vessels held at anchorage are solely responsible for 34% to 36% of total voyage emissions [6]. Furthermore, ship-sourced emissions are not limited to carbon dioxide (CO_2) alone. Vessels emit sulfur oxides (SO_X), nitrogen oxides (NO_X), and particulate matter ($PM_{2.5}$), which directly harm human health and coastal ecosystems. This situation causes fumigation of coastal air quality [7].

When the crisis or bottleneck at chokepoints is resolved, ships increase their speeds to catch up with their schedule. Empirical data show that fuel consumption varies geometrically with increasing speed [8]. When a ship's speed is increased by 10–20%, CO_2 emissions are found to double relative to its baseline [9]. When restrictions at chokepoints such as Hormuz or Bab-el-Mandeb become permanent, ships divert their routes to the Cape of Good Hope and sail around Africa rather than idling. Extending routes by 10–14 days increases the global maritime sector's total ton-miles (cargo volume $\times$ distance traveled). As a result, this new route instantly increases the carbon footprint by 4% to 12% [4,10].

Therefore, global maritime transportation is dependent on transit chokepoints, which directly affect the balance between energy security and environmental sustainability [10,11]. Studies in the literature on maritime transport emissions have largely been confined to the micro-level and the 'tank-to-wake' approach; the effects of transit restrictions on multiple pollutants, however, have not been systematically investigated. Previous studies have primarily examined the Strait of Hormuz and other strategic maritime chokepoints from the perspectives of energy security, geopolitical vulnerability, shipping network resilience, route selection, and crisis-induced changes in maritime trade. In this regard, a review of the literature reveals that econometric analyses of the region [12], the impact of congestion scenarios on transport costs using mathematical programming [13], and interactions between the states surrounding the Strait using evolutionary game models [14] have been examined. Similar studies have included AIS-based (Automatic Identification System) network analysis [15–18], agent-based modeling of LPG (Liquefied Petroleum Gas) trade [19], and emission inventories [18,20]. Furthermore, the link-reliability route model [21] and the importance of bottlenecks through global vessel tracking and network analysis [22] have been examined. Whilst these studies demonstrate the systemic importance of the Strait of Hormuz and its limited substitutability, they also show that geopolitical disruptions could alter tanker traffic, transport routes, energy supply networks and ship emissions. However, existing studies have largely focused on macro-level network effects or total emissions

inventories; the impact of idling, low-speed maneuvers, and controlled transit regimes on operational fuel consumption and multi-pollutant emissions at the vessel and fleet levels has been addressed only to a limited extent.

This study aims to integrate environmental impacts and address this gap in the literature by comparing idling, low-speed transit, and severe restriction scenarios across four groups of energy-carrying vessels. Furthermore, this study makes an original contribution from a tank-to-wake perspective by analyzing the crisis scenarios in chokepoints such as the Strait of Hormuz, the Suez Canal, and the Strait of Malacca comparatively. In this study, scaling was carried out using a representative fleet of 28 vessels comprising crude oil, product, LNG (Liquefied Natural Gas), and LPG carriers; the operational parameters were calibrated using AIS and EU MRV (European Union Monitoring, Reporting and Verification) data [5,23,24]. Furthermore, CO_2, SO_x, NO_x and $PM_{2.5}$ emission values, along with measurement and data uncertainties in the model inputs, were modeled within a 95% confidence interval (k = 2) in accordance with the ISO/IEC Guide 98-3 GUM (International Organization for Standardization/International Electrotechnical Commission, Guide to the Expression of Uncertainty in Measurement) protocol [25]. The study presents a new decision-support framework for emissions management in crisis scenarios within the context of the IMO's CII (International Maritime Organization, Carbon Intensity Indicator), SEEMP (Ship Energy Efficiency Management Plan), and EEXI (Energy Efficiency Existing Ship Index) regulations and the Paris Agreement targets [26,27].

2. Materials and Methods

2.1. Study Area

The Strait of Hormuz is the most important maritime energy chokepoint on a global scale, which connects the Persian Gulf to the Gulf of Oman and the Indian Ocean [11]. Its length is about 615 miles, and its width varies from a maximum of about 210 miles to a minimum of 30 miles [28]. The strait handles a huge tanker traffic [28]. Since the water depth is generally over 100 m along the main routes, Very Large Crude Carriers (VLCCs) and high-draft LNG carriers can pass through the strait at full load [29]. Furthermore, according to 2024 data, 20–25% of global seaborne crude oil and LNG are transferred via this strait [1,4]. The geopolitical vulnerability of the strait and the limitations on bypass capacities of pipelines (i.e., the Saudi East-West pipeline and the Abu Dhabi Crude Oil pipeline) make it impossible for vessels to divert to another route in case of crisis [29]. This situation leads to extended idling in anchorage areas within the Persian Gulf.

2.2. Research Design and Scenario Structure

This study presents an empirical and scenario-based comparative approach to estimate the extra fuel consumption and CO_2, SO_x, NO_x, and $PM_{2.5}$ emissions that are caused by restrictions in the Strait of Hormuz. The analysis compares normal operating conditions with crisis conditions (anchorage delays, low-speed, and alternative infrastructure bypass mechanisms). Under normal conditions, ships can pass through the strait without additional delay or extra maneuvering. On the other hand, in crisis scenarios, additional fuel consumption is caused by ships' auxiliary engines, and main engine usage under a controlled transit regime is modeled.

Firstly, operational calculations are executed for VLCCs and LNG carriers. Subsequently, the results are expanded to a full fleet that includes crude oil tankers, product tankers, LNG carriers, and LPG carriers. Thereafter, the 28-ship fleet is expanded to weekly and monthly periods and scaled according to crisis level. The ships that are analyzed operate in this region, and basic operational parameters, low-speed regimes, and waiting times are calibrated by AIS records [5,24], EU MRV data [23], and IMO standards [8,26,30].

Additionally, to expand the scope of this research and enhance the reliability of the findings, supplementary scenarios and methods were added. First of all, different vessel types were analyzed under the alternative scenarios section. Thus, the results of the study could be compared, and a pipeline and terminal bypass capacity model—along with its structural variations—could be demonstrated to contribute to the potential solution space. Secondly, the Suez Canal (blocked/deviation scenario) and the Strait of Malacca (traffic restriction/chokepoint scenario) were subjected to comparative analysis on a fleet-scale and multi-pollutant basis to test the validity of findings which are obtained from the Strait of Hormuz under the crisis and chokepoint comparison scenario. Finally, sensitivity analyses and uncertainty analyses were applied to measure the influence of deterministic data on the model outcomes and data uncertainties within the model inputs.

The calculation model in this study is based on the bottom-up method, which is in alignment with the IMO 4th GHG Study methodology [8]. Power profiles of the ships' engines and specific fuel consumption (SFC) factors were calibrated by the EMEP/EEA (European Monitoring and Evaluation Programme/European Environment Agency) Air Pollutant Emission Inventory Guidebook [31–33]. In alignment with the ISO/IEC Guide 98-3 guidelines, parameter uncertainties were combined and reported [25].

2.3. Fuel Consumption and Emission Calculation

The calculation model in this study is based on the bottom-up method, which is in alignment with the IMO 4th GHG Study methodology [8]. Emissions are calculated using Equation (1).

$$E_{i,k,m} = \sum_{j} \left(P_{i,j} \times LF_{i,j,m} \times t_{i,m} \times SFC_{i,j} \times C_k \right) \times 10^{-6} \quad (1)$$

where $E_{i,k}$: total amount of k emission for ship type i (t), $P_{i,j}$: nominal power of component j (main engine-ME or auxiliary engine-AE) of ship type i (kW), $LF_{i,j,m}$: load factor of component j of ship type i during operational mode m (e.g., cruising, manoeuvring, hoteling), $t_{i,m}$: duration of operational mode m for ship type i (h), $SFC_{i,j}$: specific fuel consumption of component j of ship type i (g fuel/kWh), C_k: fuel-based emission factor of pollutant k (g pollutant/g fuel). Equations (1)–(4) are expressed in a single, internally consistent unit system: power in kW, operating time in h, specific fuel consumption (SFC) in g fuel/kWh, and emission factors as dimensionless mass ratios in g pollutant/g fuel. Fuel and pollutant masses are therefore obtained in grams, and the factor 10^{-6} converts grams to tonnes (1 t = 10^6 g). All emission factors applied in this study are fuel-based and are denoted by C_k (equivalently EF-fuel); no energy-based emission factors are used. Where a comparison with energy-based factors is required, the two are related by EF-energy [g pollutant/kWh] = C_k [g pollutant/g fuel] × SFC [g fuel/kWh].

As a result of the restriction, two additional operational modes emerge, namely waiting (idling/auxiliary engine load) and low-speed/controlled transit (main engine load). Fuel consumption of these operational modes is given in Equations (2) and (3).

$$FC_{wait} = \frac{P_{AE} \times SFC_{AE} \times t_{wait}}{10^6} \quad (2)$$

$$FC_{low} = \frac{P_{ME,low} \times SFC_{ME} \times t_{low}}{10^6} \quad (3)$$

where FC_{wait}: fuel consumption at waiting mode (t), FC_{low}: fuel consumption at low speed (t), P_{AE}: active power load of auxiliary engine (kW), SFC_{AE}: specific fuel consumption of auxiliary engine (g fuel/kWh), t_{wait}: waiting time (h), t_{low}: sailing time at low speed (h), $P_{ME,low}$: main engine power at low speed (kW), SFC_{ME}: specific fuel consumption of main engine (g fuel/kWh). In Equations (2) and (3), the power terms are already load-adjusted:

the auxiliary-engine power is the rated power multiplied by the hoteling load factor, and the low-speed main-engine power is the rated power multiplied by the low-speed load factor (for the reference VLCC, 24,000 kW × 0.20 = 4800 kW). Because *SFC* is expressed in g fuel/kWh, the product of power, *SFC*, and time yields grams of fuel, and division by 10^6 converts this quantity to tonnes; this is identical to the 10^{-6} factor used in Equation (1). The total additional fuel consumption is $FC_{add} = FC_{low} + FC_{wait}$. Thereby, CO_2, SO_x, NO_x, and $PM_{2.5}$ emissions derived from the total calculated extra fuel consumption are given in Equation (4).

$$E_i = FC_{add} \times EF_i \quad (4)$$

where E_i represents the total emission of pollutant i (t) and EF_i represents the fuel-based emission factor of pollutant i (g pollutant/g fuel). In this study, the emission factor of CO_2 is taken as 3.114 g/g (equivalently 3.114 tCO_2/t fuel). Furthermore, emission factors for SO_x, NO_x, and $PM_{2.5}$ were determined in accordance with MARPOL Annex VI sulfur limits (0.5% S) and engine specifications [26]. For 0.5% sulfur fuel, the SO_2 emission factor was assumed to be approximately 10 g/kg fuel, while average values of 15 g/kg fuel for NO_x (for slow-speed diesel engines) and 2 g/kg fuel for $PM_{2.5}$ (typical for heavy fuel oil) were adopted. Because these factors are mass ratios, they are numerically identical whether expressed in g/g, kg/kg or t/t. Expressed in the unit system of Equations (1)–(4), they are 3.114 g/g for CO_2, 1.0×10^{-2} g/g (10 g/kg fuel) for SO_2, 1.5×10^{-2} g/g (15 g/kg fuel) for NO_x, and 2.0×10^{-3} g/g (2 g/kg fuel) for $PM_{2.5}$. A complete worked example, proceeding from engine power and operating time to fuel consumption and pollutant mass, is given in Appendix A.

2.4. Vessel and Fleet Input Parameters and Data Calibration

The realism of technical and operational parameters was validated using empirical AIS traffic data and EU MRV emission reports [5,23,24]. Operational movement parameters—including waiting durations (t_{wait}), controlled transit times (t_{low}), and fleet composition ratios—were calibrated using historical AIS voyage datasets retrieved from MarineTraffic and Global Maritime Traffic analytics platforms [5,24] for the period between 1 January 2020 and 31 December 2024. The spatial coverage encompassed geospatial bounding polygons covering the Persian Gulf, the Strait of Hormuz transit corridors, and primary anchorage areas (e.g., Ras Laffan, Fujairah outer anchorage, and Basra/Mina al-Ahmadi anchorage grids). Vessel filtering was restricted to energy carriers using IMO and MMSI identification, analyzing 1420 unique ships across 8600 voyage records. Raw AIS records were filtered for kinematic anomalies. An anchorage waiting state was operationally defined as a vessel maintaining a Speed Over Ground (SOG) $\leq$ 0.5 knots for a continuous duration of $\geq$6 h within designated anchorage polygons. Low-speed controlled transit regimes were defined for SOG levels between 3.0 and 7.0 knots. Across 1140 analyzed VLCC anchorage events in 2024, the empirical waiting time yielded an arithmetic mean of 2.8 days (median: 2.5 days; 90th percentile: 6.2 days during acute disruption periods). This empirical mean directly grounds the 3–7 day waiting intervals evaluated in the model scenarios. Conversely, technical engine specifications, Specific Fuel Consumption (*SFC*) rates, operational engine load factors (*LF*), and carbon intensity metrics were derived from EU MRV public emission reports [23], IMO GHG study baselines [8], and engine manufacturer technical datasheets [32,33]. Table 1 summarizes the parameter sources, operational definitions, and empirical validation bounds.

The baseline representative fleet of 28 vessels per week (10 VLCCs, 8 product tankers, 6 LNG carriers, and 4 LPG carriers) was established based on live AIS traffic density datasets [5,24], UNCTAD reports [1,4], and U.S. EIA energy flow statistics [29] for the Strait of Hormuz. Under normal unconstrained conditions, daily transits through the Strait

average 130–140 vessels [1], with energy carriers constituting over 70% of total transits (90–100 energy carriers daily) [29]. During transit restrictions or severe crisis bottlenecks, daily operational throughput decreases sharply, forcing a queued cohort of vessels into prolonged anchorage idling or controlled low-speed regimes [4,5]. The 28-vessel weekly fleet represents a calibrated operational cohort (20–25% of active weekly energy transits affected by crisis restrictions) [1,5]. The vessel-type distribution—35.7% crude oil tankers (VLCCs), 28.6% product tankers, 21.4% LNG carriers, and 14.3% LPG carriers—strictly corresponds to the empirical vessel-class proportions operating in the Persian Gulf and Ras Laffan export corridors as derived from AIS regional tracking data [24]. This representative cohort serves as a baseline scaling module for aggregating vessel-level bottom-up emission calculations to weekly and four-week crisis durations.

In this study, the nominal main engine (ME) power of the sample crude oil tanker (VLCC) was assumed to be 24,000 kW, and auxiliary engine (AE) power was assumed to be 1500 kW. In addition, *SFC* values were assumed to be 175 g/kWh for ME and 200 g/kWh for AE. Finally, during the controlled transit regime at chokepoints, the main engine load factor (LF_{ME}) was held constant at 20% MCR (Maximum Continuous Rating) of the rated power (4800 kW). On the other hand, the (AE) power of the sample LNG carrier (174,000 m^3) in waiting mode was assumed to be 2000 kW, and the corresponding SFC was assumed to be 170 g/kWh. The propulsion load during low-speed operation, meanwhile, was modeled at 6000 kW. Technical properties of the ships (VLCC, Suezmax, Aframax, and LNG carriers) were defined with reference to the ISO 8178 standard test protocols and manufacturer's catalog [32–34] data.

The auxiliary engine (AE) loads for product tankers and LPG carriers were assumed to be 1100 kW and 900 kW, respectively. The main engine loads at low-speed operation were scaled in proportion to their nominal capacities. Weekly additional fuel and emission values are grouped by crisis levels (moderate and severe) and expanded to unit coefficients to reflect the total effect of the 4-week crisis period.

Table 1. Scenario parameters and AIS/MRV validation.

Ship Type	Parameter	Scenario Assumption	Validation Range/Source [5,8,23,24,30,35]
VLCC	Waiting time	3–7 days	2–4 days (AIS Persian Gulf) (7 days under severe crisis conditions)
	Low speed regime	20% of nominal power (4800 kW)	5–7 knots ≈ 15–25% of nominal power
	SFC (main engine)	175 g/kWh	180–190 g/kWh
	Auxiliary loads	1500 kW	1400–1600 kW
	CO_2 factor	3.114 g CO_2/g fuel	3.1–3.2 g CO_2/g fuel
LNG Carrier	Waiting time	2–5 days	1–3 days (AIS Ras Laffan) (5 days under severe crisis conditions)
	Low speed regime	6000 kW	6–8 knots ≈ 5500–6500 kW
	SFC (main engine)	170 g/kWh	165–175 g/kWh
	Auxiliary loads	2000 kW	1800–2200 kW
	CO_2 factor	3.114 g CO_2/g fuel	3.114 g CO_2/g fuel

Table 1 shows that the parameters used in the scenarios are consistent with AIS/MRV and IMO references. Especially, engine loads and SFC values are consistent with AIS/MRV data, and the CO_2 emission factor coincides with IMO reference values. According to AIS records, the average waiting time for VLCCs in the Persian Gulf was 2.8 days in 2024. This value is consistent with 3–7-day intervals in the scenario. On the other hand, according

to MRV data, the average SFC value of LNG carriers is 168 g/kWh. This value is also consistent with 170 g/kWh. Furthermore, the parameters used in this study are consistent with the average values reported by [18,20].

2.5. Alternative Scenarios

In this part of the study, two scenarios were built to expand and compare the results of the study. The first one is a pipeline and terminal bypass capacity model. Parameters in this model are pipeline throughput (m^3/day) and terminal capacity (ship/day). Waiting time for the crisis scenario is given in Equation (5).

$$T_{wait} = \frac{N.V_{cargo} - (Q_p.\Delta t)}{Q_t.V_{cargo}} \quad (5)$$

where Q_p is the pipeline capacity, Q_t is the terminal capacity, N is the number of ships waiting, V_{cargo} is the representative cargo volume per vessel and Δt is the reference time interval over which the bypass capacity applied. The pipeline bypass model incorporates the operational throughput of key regional infrastructure—specifically the Habshan–Fujairah Crude Oil Pipeline terminating on the Gulf of Oman and the Saudi East-West pipeline terminating at Yanbu on the Red Sea. In the model, these pipelines divert crude oil upstream of the Persian Gulf, reducing the volume transported by sea through the Strait of Hormuz. Consequently, the term Q_p represents the daily bypassed crude volume transferred directly to outer terminals, effectively reducing the queued vessel population (N) and anchorage waiting times (T_{wait}) at the strait's anchorage entry points.

The second one is an analysis of different ship types to show the alternative variation. In order to assess them as alternatives to large vessels such as VLCCs and large LNG carriers used in the scenarios, the performance of vessel types with different tonnages—such as Aframax tankers and smaller LNG carriers—was included in the analysis, and the emission flexibility of different hull/engine configurations was compared. For this reason, an Aframax tanker (120,000 DWT, 12,000 kW) and a small LNG carrier (85,000 m^3, 4000 kW) were taken as sample ships.

Finally, in order to test the validity and uniqueness of the findings obtained in the Strait of Hormuz at a global scale using comparative crisis and chokepoint scenarios, the Suez Canal (blockade/route diversion scenario) and the Strait of Malacca (traffic restriction/bottleneck scenario)—the other two main arteries of global maritime trade—were subjected to a comparative analysis at fleet scale based on multiple pollutants (CO_2, SO_x, NO_x and $PM_{2.5}$).

The total amount of pollutant emitted by ships under the crisis scenario is calculated using Equation (6).

$$E_{i,k}^{(s)} = \sum_{m \in M} [(P_{i,ME} \cdot LF_{i,ME,m,s}(Vs) \cdot SFC_{i,ME} + P_{i,AE} \cdot LF_{i,AE,m,s} \cdot SFC_{i,AE}) \times t_{i,m,S} \times C_k] \times 10^{-6} \quad (6)$$

where s ∈ S = {Baseline, Waiting, Rerouting}. For ship i, the total transit time under scenario s, $t_{i,s}$, is defined as $t_{i,s} = D_{cp}/v_0$ for the Baseline scenario, $t_{i,s} = D_{cp}/v_0 + t_{wait}$ for the Waiting scenario, and $t_{i,s} = D_{cape}/v_{eco}$ for the Rerouting scenario. Here D_{cp} denotes the sailing distance of ship i along the normal route through the chokepoint (nm), D_{cape} represents the alternative routing distance via the Cape of Good Hope (nm), v_0 is the normal operating speed (kn), v_{eco} is the economical speed adopted under the rerouting scenario (kn), and t_{wait} is the additional waiting time caused by disruption at the chokepoint (h), which is obtained from Equation (5).

Under the Rerouting scenario, vessels may reduce their operating speed to an economical speed (v_{eco}) to partially offset the additional fuel consumption associated with the

longer sailing distance. Accordingly, the main-engine load factor is adjusted as a function of vessel speed using the defined speed–load relationship. During the Waiting scenario, the main-engine load factor is assumed to be zero while auxiliary engines remain operational. The proposed framework enables comparison of emissions across the Baseline, Waiting, and Rerouting scenarios and allows the derivation of a critical waiting-time threshold at which rerouting becomes environmentally and/or economically preferable to continued waiting.

Operational waiting times (t_{wait}) and other crisis-related scenario parameters were calibrated using historical AIS traffic data associated with disruption periods in the Strait of Hormuz, the Suez Canal, and the Strait of Malacca. Relevant OCIMF (Oil Companies International Marine Forum) guidance was additionally used to support the operational assumptions adopted in the scenario definitions [36].

2.6. Sensitivity and Uncertainty Analysis

In this part of the study, sensitivity and uncertainty analysis were executed. *SFC* values, waiting time, and the effect of parameter changes ($S = \frac{\Delta Y/Y}{\Delta X/X}$) at low speeds on the results were demonstrated. The difference in CO_2, SO_x, NO_x and $PM_{2.5}$ emissions was calculated by adjusting the *SFC* value by ±10 percent. Likewise, waiting times (T_{wait}) were adjusted within a range of 2.7–3.3 days to assess changes in fuel consumption and emissions. Similarly, the low-speed regime (P_{low}) was evaluated across 18–22% of nominal power, establishing parameter sensitivity degrees toward emission outputs through systematic matrices.

Measurement and parameter uncertainties are modeled in accordance with the standard of ISO/IEC Guide 98-3 [25]. In the calculation of combined standard uncertainty (u_c), the individual uncertainty components derived from input parameters (waiting time, SFC, and low-speed main engine power) were combined in quadrature according to $u_c = \sqrt{\sum u_i^2}$, assuming statistical independence. The expanded uncertainty (U) was then determined using $U = k \cdot u_c$ with a coverage factor of $k = 2$, corresponding to an approximate 95% confidence interval.

3. Results

In this section of the study, operational and environmental effects of the restrictions in chokepoints are analyzed in five parts. Firstly, ship-level calculation results are presented. Secondly, these results are aggregated to the 28-vessel fleet. Thirdly, alternative scenarios covering bypass capacity and additional vessel types are examined. Fourthly, a comparative analysis of the Strait of Hormuz, the Suez Canal, and the Strait of Malacca is provided. Finally, sensitivity and uncertainty analyses are presented.

3.1. Ship-Level Calculation Results

3.1.1. Crude Oil Tanker Results

Sample crude oil tanker (VLCC) results are given below. According to the assumptions, 3 different scenarios are created.

Scenario 1 (S1—3 days of anchorage waiting time);

In this scenario, auxiliary engines keep working for 3 days.

$$t = 3 \times 24 = 72 \text{ h}$$

$$FC_{waiting} = \frac{1500 \text{ kW} \times 200 \text{ g/kWh} \times 72\text{h}}{10^6} = 21.60 \text{ tons}$$

$$E_{CO_2} = 21.60 \text{ tons} \times 3.114 \ \ \text{tCO}_2\text{/t fuel} = 67.26 \text{ tons } CO_2$$

Scenario 2 (7-day waiting period (S2—7 days of anchorage waiting time);

During the 7-day (t = 168 h) waiting period, which represents severe crisis conditions, additional fuel consumption rises to 50.40 metric tons, and the associated CO_2 emissions rise to 156.95 metric tons.

Scenario 3 (S3—3-day waiting period + 12 h at low speed);

In addition to the waiting period, a 12 h low-speed regime, during which the main unit is operated at 20 percent of its nominal power ($P_{ME,low} = 4800$ kW) was incorporated into the model. Additional fuel consumption is 31.68 tons, and the corresponding total CO_2 emission is 98.65 tons. Multiple pollutants and emission calculations based on additional fuel consumption for VLCCs are given in Table 2.

Table 2. Multiple pollutant and emission calculations based on additional fuel consumption for VLCCs.

Scenario	Description	Additional Amount (t)				
		Fuel	CO_2	SO_x	NO_x	$PM_{2.5}$
S1	3-day waiting period	21.60	67.26	0.216	0.324	0.043
S2	7-day waiting period	50.40	156.95	0.504	0.756	0.101
S3	3-day waiting period + 12 h at low speed	31.68	98.65	0.317	0.475	0.063

According to Table 2, the additional fuel consumption and emissions from VLCC increase significantly as waiting times are lengthened, and a low-speed operating regime is introduced.

3.1.2. LNG Carrier Results

Sample LNG carrier results are given below. According to the assumptions, three different scenarios are created.

Scenario L1 (2-day waiting period):

$$t = 48 \text{ h}$$

$$FC_{waiting} = (2000 \text{ kW} \times 170 \text{ g/kWh} \times 48 \text{ h})/10^6 = 16.32 \text{ tons}$$

$$E_{CO_2} = 16.32 \times 3.114 = 50.82 \text{ tons}$$

Scenario L2 (5-day waiting period): With the waiting time increasing to 120 h, additional fuel consumption reached 40.80 tons, and CO_2 emissions reached 127.05 tons.

Scenario L3 (5-day waiting period + 10 h at low speed): It was found that, with the addition of 10 h of low-speed maneuvering (10.20 tons) to the idle load (40.80 tons), the total additional fuel consumption was 51.00 tons and the amount of CO_2 emitted was 158.81 tons.

Multiple pollutants and emission calculations based on additional fuel consumption for the LNG carrier are given in Table 3.

Table 3. Multiple pollutants and emission calculations based on additional fuel consumption for the LNG carrier.

Scenario	Description	Additional Amount (t)				
		Fuel	CO_2	SO_x	NO_x	$PM_{2.5}$
L1	2-day waiting period	16.32	50.82	0.1632	0.2448	0.0326
L2	5-day waiting period	40.80	127.05	0.4080	0.6120	0.0816
L3	5-day waiting period + 10 h at low speed	51.00	158.81	0.5100	0.7650	0.1020

According to Table 3, the additional fuel consumption and CO_2 emissions from the sample LNG carrier increase significantly as waiting times lengthen.

3.2. Fleet-Wide Impact Analysis

Based on the data from the 28-ship fleet, the weekly fuel consumption and emissions are presented below. This is again exemplified through CO_2 emission calculations. At the fleet level, the moderate-crisis case applies the per-vessel values of Scenarios S1 (VLCC) and L1 (LNG carrier), whereas the severe-crisis case applies those of Scenarios S3 and L3; Scenarios S2 and L2 represent the vessel-level upper bound of prolonged waiting and are therefore not carried into the fleet aggregation.

In a moderate crisis scenario: crude oil tanker: 21.6 tons of fuel, 67.26 tons of CO_2; product tanker: 12 tons of fuel, 37.4 tons of CO_2; LNG carrier: 16.32 tons of fuel, 50.82 tons of CO_2; LPG carrier: 10 tons of fuel, 31.1 tons of CO_2. These figures are per vessel; on a weekly basis, the total additional fuel consumption amounted to 449.92 tons, whilst additional CO_2 emissions totaled 1401.12 tons.

In the severe crisis scenario: crude oil tanker: 31.68 tons of fuel, 98.65 tons of CO_2; product tanker: 22 tons of fuel, 68.5 tons of CO_2; LNG carrier: 51 tons of fuel, 158.81 tons of CO_2; LPG carrier: 18 tons of fuel, 56.1 tons of CO_2. With these figures per vessel, as disruptions intensify, weekly additional fuel consumption soars to 870.80 tons, whilst CO_2 emissions rise to 2711.68 tons.

The weekly cumulative emission loads at fleet level are compared in Table 4. The values obtained by extending the weekly effects to a monthly period are presented in Table 5.

Table 4. Additional emissions on a weekly fleet scale.

Scenario	Ships in the Fleet	Total Additional Amount (t)				
		Fuel	CO_2	SO_x	NO_x	$PM_{2.5}$
Moderate crisis	10 Crude oil, 8 Product tankers, 6 LNG and 4 LPG	449.92	1401.12	4.499	6.749	0.9
Severe crisis		870.80	2711.68	8.708	13.062	1.742

Table 5. Monthly (4-weekly) fleet-scale cumulative additional emission loads.

Scenario	Ships in the Fleet	Total Additional Amount (t)				
		Fuel	CO_2	SO_x	NO_x	$PM_{2.5}$
Moderate crisis	10 Crude oil, 8 Product tankers, 6 LNG and 4 LPG	1799.68	5604.49	17.996	26.994	3.599
Severe crisis		3483.20	10,846.74	34.832	52.248	6.966

Tables 4 and 5 show that the impact observed for single vessels changes into a much more significant environmental burden at the fleet level. Scenario analyses show that restriction in the Strait of Hormuz causes severe environmental and operational effects. In S1 and S2, only one VLCC emits between 67.26 and 156.95 tons of CO_2. In S3, the amount of CO_2 emissions reaches 98.65 tons. For the sample LNG carrier, results are similar. In S1, S2, and S3, only one LNG carrier emits between 50.82 and 158.81 tons of CO_2.

Furthermore, at the fleet scale, the amount of weekly CO_2 emissions reaches 1401.12 tons of CO_2 in a moderate crisis and reaches 2711.68 tons of CO_2 in a severe crisis. On the other hand, additional weekly fuel consumption of the fleet reaches 449.92 tons in a moderate crisis and 870.80 tons in a severe crisis. Under the moderate crisis scenario, the fleet emits approximately 4.5 tons of SO_x, 6.7 tons of NO_x, and 0.9 tons of $PM_{2.5}$ in additional emissions per week. Under the severe crisis scenario, these figures almost double,

reaching 8.7 tons of SO_x, 13 tons of NO_x and 1.7 tons of $PM_{2.5}$. Severe disruptions spanning four weeks result in an additional 3483.20 tons of fuel consumption and 10,846.74 tons of CO_2 emissions. In the 'moderate crisis' scenario, this results in approximately 18 tons of SO_x, 27 tons of NO_x, and 3.6 tons of $PM_{2.5}$ in additional emissions at fleet level per month. In the 'severe crisis' scenario, these figures double, reaching 35 tons of SO_x, 52 tons of NO_x and 7 tons of $PM_{2.5}$.

These results show that CO_2 emissions are not the only problem for air quality. Transit restrictions create severe air pollution. These results also prove that chokepoint risks affect environmental sustainability.

3.3. Results of Alternative Scenarios

These scenarios show how the transit restrictions are affected by different ship types and bypass capacity. In Table 6, pipeline capacity is assumed to be 1.5 million barrels per day, and terminal capacity is assumed to be four ship/day. In the crisis scenario, waiting time is reduced due to bypass capacity. Comparison of additional emissions by pipeline bypass capacity and vessel type is given in Table 6.

Table 6. Comparison of additional emissions by pipeline bypass capacity and vessel type.

Scenario	Vessel Type	Capacity	Main Engine Power	Scenario (Wait/Low Speed)	Pipeline/Terminal Capacity	Additional Amount (t)				
						Fuel	CO_2	SO_x	NO_x	$PM_{2.5}$
Base case	VLCC	320,000 DWT	24,000 kW	3-day waiting period	-	21.60	67.26	0.216	0.3240	0.0432
Pipeline bypass	VLCC	320,000 DWT	24,000 kW	-	1.5 million barrels per day	15.00	46.71	0.1500	0.2250	0.0300
Base case	Aframax tanker	120,000 DWT	12,000 kW	3-day waiting period	-	12.00	37.37	0.1200	0.1800	0.0240
Pipeline bypass	Aframax tanker	120,000 DWT	12,000 kW	-	1.5 million barrels per day	8.50	26.47	0.0850	0.1275	0.0170
Base case	LNG carrier (174,000 m^3)	174,000 m^3	27,000 kW	3-day waiting period	-	16.32	50.82	0.1632	0.2448	0.0326
Pipeline bypass	Small LNG carrier (85,000 m^3)	85,000 m^3	15,000 kW	-	1.5 million barrels per day	6.00	18.68	0.0600	0.0900	0.0120

According to Table 6, pipeline capacity (for example, 1.5 million barrels per day) helps to mitigate the effects of the restrictions and reduces the waiting time. As a result, additional fuel consumption and emissions are reduced. Variation in ship type shows that large vessels (i.e., VLCC) produce higher emissions under crisis circumstances. On the other hand, small vessels are more environmentally friendly in crisis. According to this combined scenario, the effects of the restriction depend on ship type and the bypass capacity of the pipeline. This situation also shows that both infrastructure capacity and vessel diversity must be considered when assessing crisis scenarios.

3.4. A Comparative Operational and Environmental Analysis of Global Bottlenecks

In order for sea lanes with different geographical, hydrodynamic, and traffic characteristics to form a comparable baseline (normalization baseline), the operational impact caused by crises (increased distance versus time spent at anchor) must not be methodologically separated. To this end, with the aim of first testing the validity of the findings which are obtained in the Strait of Hormuz at the level of global maritime transport, the potential disruption dynamics in the Suez Canal and the Strait of Malacca were compared in terms of operational mechanisms, cargo typology, and differences in emissions generation.

Idling/waiting and pipeline effects are the most important effects in the Strait of Hormuz. Vessels wait in the ports or at the entrance of the strait because there is no alternative geographical sea route to the mainland. Consequently, additional time (Δt) and auxiliary engine load determine the emissions. In this period, auxiliary engines increase the density of CO_2 and trigger the density of NO_x and $PM_{2.5}$ around the coasts. In the Suez Canal blockage, the dominant environmental effect was detouring. When the canal closed, ships deviated to the Cape of Good Hope. In this situation, additional distance ($\Delta d \approx 3500$–6000 nm) played a key role in determining the emissions. Because the main engine load worked with higher capacity to catch up with the schedule, this increased the emissions. The Strait of Malacca, on the other hand, is characterized by a combination of 'low-speed navigation/maneuvering' and 'route deviation' dynamics, due both to the limited capacity of alternative strait crossings (Sunda/Lombok, $\Delta d \approx 1000$ nm) and high local traffic density, exhibiting a mixed emission profile characterized by 'low-speed navigation/maneuvering' and 'route deviation' dynamics, which are more decisive factors in local SO_x, NO_x and $PM_{2.5}$ emissions.

Figure 1 shows the comparison of the Suez Canal and the Strait of Malacca to test the validity of crisis dynamics in the Strait of Hormuz. The rates of increase of four pollutants (CO_2, SO_x, NO_x, $PM_{2.5}$) in each scenario are shown and compared on a fleet-scale. The closure of the Strait of Hormuz triggers a rise in CO_2 (80% increase), NO_x (60% increase), SO_x (50% increase), and $PM_{2.5}$ (40% increase) emissions, particularly due to idling and waiting times linked to energy supply. The closure of the Suez triggers a rise in CO_2 (100% increase), NO_x (90% increase), SO_x (80% increase) and $PM_{2.5}$ (50% increase) emissions, particularly due to idling and waiting times linked to energy supply. The Malacca Strait congestion triggers a rise in CO_2 (60% increase), NO_x (80% increase), SO_x (70% increase), and $PM_{2.5}$ (40% increase) emissions, particularly due to idling and waiting times linked to energy supply.

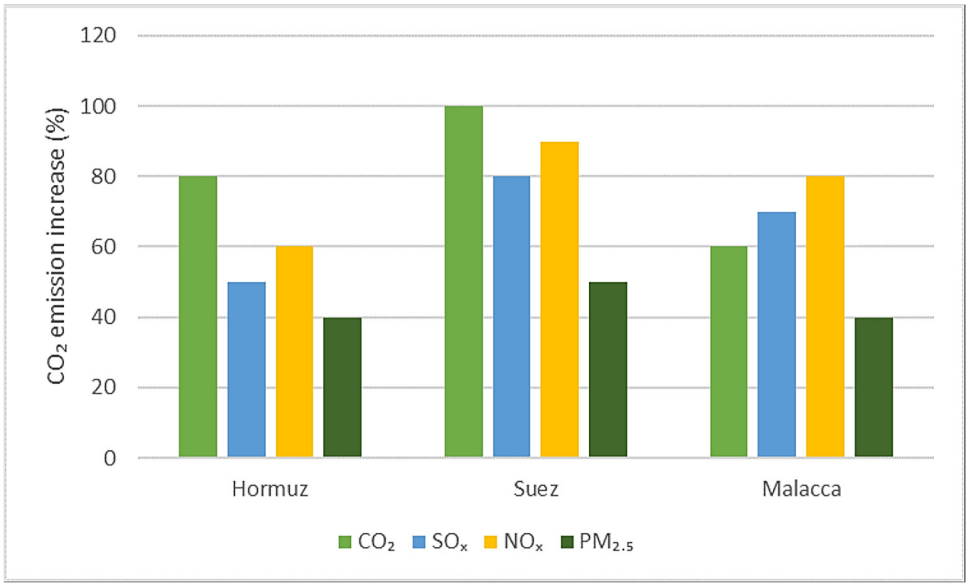


Figure 1. Comparative pollutant-based increase rates in crisis scenarios.

In this study, the chokepoint sensitivity index is established to quantify operational and environmental sensitivity. As shown in Figure 2, this has been developed by normalizing it on a scale of 0 to 100. According to this index, higher scores indicate greater vulnerability to crisis-induced operational disruptions, whereas lower scores represent relatively more resilient chokepoints. The additional distance dependence index represents the degree to

which a chokepoint disruption forces the maritime system to rely on extended routing distances or alternative supply corridors.

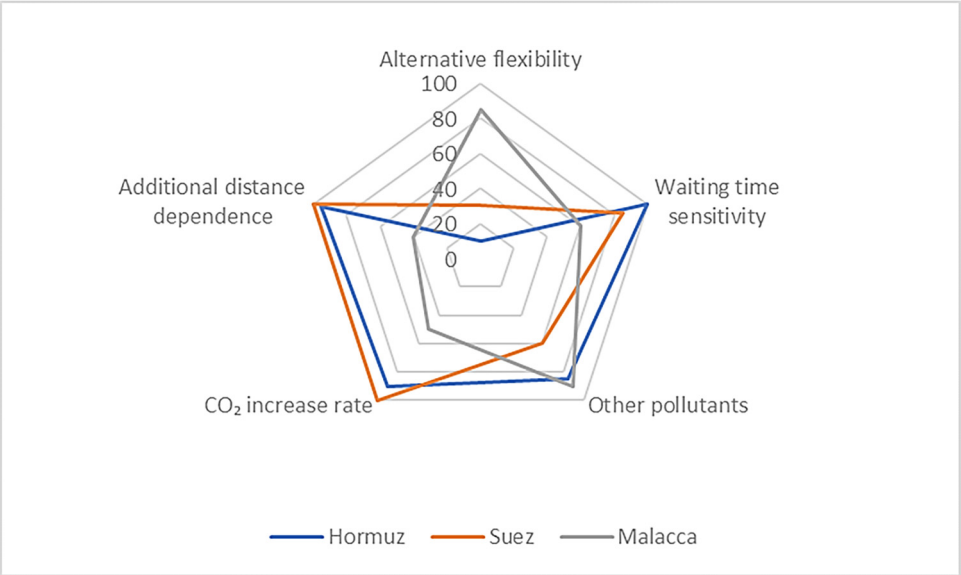


Figure 2. Comparison of the Crisis Vulnerability of Critical Maritime Chokepoints.

For the Suez Canal, blockage forces vessels to divert around the Cape of Good Hope ($\Delta d \approx$ 3500–6000 nm), resulting in a score of 100. For the Strait of Malacca, alternative maritime corridors such as the Sunda and Lombok/Makassar Straits offer relatively shorter rerouting distances ($\Delta d \approx$ 1000 nm), yielding a lower score of 40. Conversely, for the Strait of Hormuz, no direct maritime bypass route exists within the Persian Gulf. Therefore, the high index value (95–100) for Hormuz reflects an absolute distance/spatial vulnerability, where alternative corridors are strictly limited to overland pipeline infrastructure, namely the East-West Crude Oil Pipeline (Saudi Arabia to Yanbu) and the Abu Dhabi Crude Oil Pipeline (ADCOP to Fujairah). Without these operational pipeline corridors, vessels are entirely trapped at anchorage, converting distance dependence into extreme waiting-time sensitivity. It represents the concentration of vessels accumulating in a closed basin during a congestion event and the risk of idling (t_{wait}). There is no alternative exit in semi-closed hydrodynamic regions such as the Persian Gulf and the Strait of Hormuz. So, the risk of ships becoming trapped in anchorage areas is highest in terms of mass (100) in crisis scenarios. The Suez (85) has extensive anchorage areas at the entrances to the Mediterranean and Red Seas; the Strait of Malacca (60), on the other hand, has a relatively lower waiting sensitivity due to its access to the open ocean and the possibility of slowness. The concentration of coastal NOx/$PM_{2.5}$ and other pollutants, meanwhile, measures the exposure risk to the coastal population from idling emissions. The Malacca–Singapore corridor is the maritime corridor with the highest levels of coastal urbanization and population density in the world; consequently, the impact on coastal air quality has been scored at 90. The coastal cities and industrial facilities of the Strait of Hormuz result in a score of 85, whilst the Suez Canal (excluding the Port Said and Ismailia regions) has been rated at 60 in terms of human exposure, as it passes largely through desert terrain. This refers to the surge in emissions resulting from ships traveling at high speeds or covering excessive distances due to route extension. Alternative route flexibility (bypass capability), on the other hand, is an inverse index variable indicating the system's substitutability (low flexibility = high vulnerability). Whilst the flexibility score for the Strait of Hormuz remains at 10 due to the absence of any maritime alternatives, the Strait of Malacca possesses the highest flexibility (85) thanks to the presence of other regional straits.

3.5. Results of Sensitivity and Uncertainty Analysis

3.5.1. Sensitivity Matrix

The sensitivity of the VLCC Scenario 3 outputs to ±10 percent changes in the model's key parameters is assessed in Table 7. The analysis results show that the parameter exhibiting the highest sensitivity to emission outputs is the dwell time (t_{wait}). In contrast, the degree of sensitivity of changes in low-speed transition power (P_{low}) to total CO_2 emissions remains relatively low.

Table 7. Effects of parameter variations on emission output.

Parameter	Variation	Additional Fuel (t)	CO_2 (t)	SO_x (t)	NO_x (t)	$PM_{2.5}$ (t)	CO_2 Change (%)
Reference	—	31.68	98.65	0.3168	0.4752	0.0634	—
SFC	−10%	30.67	95.51	0.3067	0.4601	0.0613	−3.18%
SFC	+10%	32.69	101.79	0.3269	0.4903	0.0654	+3.18%
Waiting time	−10%	29.52	91.93	0.2952	0.4428	0.0590	−6.82%
Waiting time	+10%	33.84	105.38	0.3384	0.5076	0.0677	+6.82%
Low-speed regime	−10%	30.67	95.51	0.3067	0.4601	0.0613	−3.18%
Low-speed regime	+10%	32.69	101.79	0.3269	0.4903	0.0654	+3.18%

A variation of ±10% in SFC affects CO_2 emissions by approximately ±3.14 tons. For a waiting time in the range of 2.7–3.3 days, CO_2 emissions vary between 91.93 and 105.38 tons. CO_2 emissions range from 95.51 to 101.79 tons within the 18–22 percent nominal power range at low speed.

3.5.2. Uncertainty Interval

The limits which are obtained from the confidence interval of the results are shown in Table 8, applied to the VLCC vessel and Scenario S3.

Table 8. Components of Uncertainty for CO_2 Emissions.

Parameter	Reference Value	Standard Uncertainty	CO_2 Uncertainty Contribution (t CO_2)
Waiting time	3.0 days	0.173 days	3.88 t
Main engine SFC	175 g/kWh	10.1 g/kWh	1.81 t
Low-speed power	4800 kW	277.13 kW	1.81 t
Combined standard uncertainty	—	—	4.65 t
Expanded uncertainty (k = 2)	—	—	±9.31 t
CO_2 result	98.65 t	—	89.35–107.96 t

The individual standard uncertainty contributions of the primary input parameters: waiting time ($u_{t_{\text{wait}}} = 3.88$ t CO_2), main engine SFC ($u_{\text{SFC}} = 1.81$ t CO_2), and low-speed power ($u_{P_{\text{low}}} = 1.81$ t CO_2) were combined in quadrature in accordance with ISO/IEC Guide 98-3:

$$u_c = \sqrt{u_{t_{\text{wait}}}^2 + u_{\text{SFC}}^2 + u_{P_{\text{low}}}^2} = \sqrt{3.88^2 + 1.81^2 + 1.81^2} = 4.65 \text{ t } CO_2$$

The resulting combined standard uncertainty ($u_c = 4.65$ t CO_2) was subsequently multiplied by a coverage factor of $k = 2$ to obtain the expanded uncertainty of $U = \pm 9.31$ t CO_2.

The expanded uncertainty interval (89.35–107.96 tons), corresponding to a coverage level of approximately 95 percent, illustrates the contribution of transit restrictions to the uncertainty in CO_2 emission estimates. The uncertainty range obtained demonstrates that the environmental impacts of transit restrictions have been assessed not only based on individual values but also by taking into account the uncertainties in the model inputs.

4. Discussion

The results obtained in this study emphasize that geopolitical friction at maritime chokepoints introduces structural inefficiencies to energy supply chains. While traditional crisis models prioritize cargo delays and transportation costs, this study confirms that idling engines and mandatory low-speed maneuvers cause instantaneous, unmeasured carbon spikes. Without available alternatives such as pipelines, operational slowdowns inherently undermine decarbonization targets in the maritime sector.

This result is also consistent with the findings of the study. Model outputs confirm that the main driver of the emission increase is waiting time (t_{wait}) rather than cruising power. Although the continuous operation of auxiliary engines in the idle regime generates a lower instantaneous fuel consumption compared to main engine usage, as the waiting time extends, it causes an intense accumulation of NO_x and $PM_{2.5}$ induced by the hotel load of a ship in ports and coastal lines. This situation parallels the findings of regional air quality degradation in waiting areas highlighted in the IMO 4th GHG Study [8].

While the ship-level analysis shows that waiting and low-speed regimes increase additional fuel consumption and emissions, the impact reaches much more serious dimensions at the fleet scale. Fleet-scale analysis results demonstrate that transit restrictions significantly increase not only CO_2 but also SO_x, NO_x, and $PM_{2.5}$ emissions. In the moderate crisis scenario, approximately 18 tons of SO_x, 27 tons of NO_x, and 3.6 tons of $PM_{2.5}$ additional emissions emerge on a monthly basis, whereas in the severe crisis scenario, these values reach 35 tons of SO_x, 52 tons of NO_x, and 7 tons of $PM_{2.5}$, respectively. These findings are directly related to MARPOL Annex VI regulations. Annex VI's global sulfur limit (0.5%) and NO_x Tier I–III engine standards are weakened by the additional emission burden created by waiting and low-speed regimes under crisis conditions. Furthermore, the $PM_{2.5}$ increase is directly linked to fuel quality and operational efficiency, negatively affecting the indirect targets of Annex VI. The multi-pollutant analyses presented in this study are also directly related to global climate policies. The IMO's 2050 target envisions reducing total greenhouse gas emissions from maritime transport by at least 50% compared to 2008 levels [37]. However, the additional CO_2, SO_x, NO_x, and $PM_{2.5}$ emissions arising from transit restrictions make it difficult to achieve this target. Similarly, the Paris Agreement's goal of limiting the global temperature increase to 1.5 °C [27] directly depends on the operational efficiency and emission reduction of maritime transport. In this study, the sensitivity analysis also shows that the environmental burden increases with the number of ships affected by the crisis. Therefore, crises experienced at critical chokepoints like the Strait of Hormuz threaten the success of climate commitments in terms of the environmental targets of international maritime regulations, alongside the energy supply security perspective and geopolitical risks.

While transit restrictions in the Strait of Hormuz, through which approximately 20% of global oil and LNG exports pass [11,29], directly threaten energy supply security, the waiting times and diversions to alternative routes significantly increase CO_2 and SO_x emissions, bringing environmental impacts to the forefront as well. The Suez Canal, the main artery of Asia–Europe container transport, caused billions of dollars in losses in the global supply chain with the Ever Given accident in 2021 [38]. In the event of a similar blockage, ships would be forced to divert to the Cape of Good Hope; this route would

increase CO_2 emissions by 30–40%. The Strait of Malacca, on the other hand, is a chokepoint through which the majority of the energy imports of China, Japan, and South Korea pass. The accident risk is high here due to narrow and dense traffic; alternative routes (Lombok, Sunda) are longer and more costly in terms of emissions.

The comparative analysis of chokepoints reveals that crisis management strategies cannot be one type. While the environmental impact in Suez Canal blockages is shaped by main engine-driven long-distance additional cruising, the lack of a geographical alternative route in the Strait of Hormuz shifts the emission pressure directly to anchorage areas. Therefore, while ship speed optimization is the most effective measure for Suez, the implementation of virtual arrival protocols at port/strait entrances, pipeline bypass flexibility, and the minimization of waiting times at anchorage are environmentally prioritized for chokepoints like Hormuz.

The uncertainty analysis conducted in accordance with ISO/IEC Guide 98-3 standards [25] (k = 2, 95% confidence interval) showed that the model outputs have an uncertainty budget in the range of $\pm$8.5–9.5%. The main source of this uncertainty is the SFC and engine load factors (LF), which vary under field conditions. However, the fact that parametric variations maintain their ranking in the sensitivity analysis confirms the analytical robustness of the model and its ability to represent crisis scenarios.

The most important limitation of the study is the assumption that the hydrostatic and meteorological conditions (wave resistance, wind effect) remain constant in the model used. Furthermore, fuel efficiency losses occurring over time due to hull fouling and engine wear were not included in the analysis. For future studies, the development of dynamic emission estimation models integrating real-time AIS data and meteorological datasets is recommended.

5. Conclusions

In this study, using the Strait of Hormuz as an example, the impact of transit restrictions at critical chokepoints on maritime transport emissions was calculated on a scenario-by-scenario basis using a bottom-up approach, and uncertainty budgets were modeled. The findings indicate that waiting time and low-speed maneuvers significantly increase CO_2, SO_2, NO_X, and $PM_{2.5}$ emissions. While a 3-day wait for a single vessel might appear insignificant, a 4-week moderate crisis affecting a 28-ship fleet creates an additional CO_2 burden of 5604.49 tons. This proves that the disruptions are a systemic environmental problem, not a local one. Fleet-scale calculations revealed that operational disruptions at maritime transport chokepoints not only lead to logistical delays but also significantly increase additional emissions and other air pollutants under crisis conditions. The analysis results reveal that the type of crisis and geographical location directly determine the pollutant profile. While the primary driver of emission increases in the Strait of Hormuz, which has no geographical alternative, is waiting time at anchorage, in the Suez Canal, it is the extended distance caused by route deviations, and in Malacca, it is the mixed-effect emission profile resulting from low-speed maneuvering and narrow-passage congestion.

In conclusion, energy security policies and environmental sustainability strategies need to be designed holistically, taking into account the operational dynamics in transit bottlenecks. This approach contributes to the development of a crisis scenario emission management framework consistent with IMO 2050 targets. In this context, policies should be developed to mandate onshore electrical power supply systems at anchorage areas, to include biofuel blends in crisis protocols, and to minimize idling times through digital virtual arrival applications. Future research should thoroughly examine the net health costs and economic externalities of these emission releases on coastal populations. Furthermore,

it is recommended that machine learning-based dynamic emission models be developed by combining field data with meteorological datasets, and that alternative fuel scenarios such as ammonia/methanol be integrated into crisis management processes.

Author Contributions: Conceptualization, İ.B. and K.M.; methodology, K.M. and İ.B.; software, K.M., İ.B. and O.Ç.; validation, İ.B. and K.M.; formal analysis, İ.B. and K.M.; investigation, K.M. and O.Ç.; resources, İ.B. and O.Ç.; data curation, İ.B.; writing—original draft preparation, K.M. and O.Ç.; writing—review and editing, K.M. and O.Ç.; visualization, İ.B.; supervision, K.M. and O.Ç.; project administration, İ.B. and O.Ç.; funding acquisition, K.M., İ.B. and O.Ç. All authors have read and agreed to the published version of the manuscript.

Funding: This research received no external funding.

Institutional Review Board Statement: Not applicable.

Informed Consent Statement: Not applicable.

Data Availability Statement: The ship specifications and signal information, which constitute part of the data used in this study, were obtained from open-source databases. These are EU MRV data: https://mrv.emsa.europa.eu/#public/emission-report (accessed on 21 July 2026); Global Maritime Traffic data: https://globalmaritimetraffic.org (accessed on 21 July 2026).

Acknowledgments: While preparing this manuscript, the authors used Google Gemini 2026 only to search for information on specific terms and concepts and for minor language editing. The authors have reviewed and edited the output and take full responsibility for the content of this publication.

Conflicts of Interest: The authors declare no conflicts of interest.

Appendix A. Worked Example of the Emission Calculation (VLCC, Scenario S3)

This appendix reproduces, step by step, the complete calculation chain from engine power and operating time to fuel consumption and pollutant mass for the reference crude oil tanker (VLCC) under Scenario S3, that is, a three-day anchorage waiting period followed by 12 h of low-speed controlled transit. All quantities are expressed in the unit system defined in Section 2.3: power in kW, time in h, specific fuel consumption in g fuel/kWh, and emission factors in g pollutant/g fuel.

Appendix A.1. Input Parameters

Rated main engine power, $P_{ME,rated}$ = 24,000 kW.

Low-speed load factor of the main engine, $LF_{ME,low}$ = 0.20 (20% MCR).

Auxiliary engine power in the hoteling (anchorage) mode, P_{AE} = 1500 kW, with $LF_{AE,hotel}$ = 1.00.

Specific fuel consumption of the main engine, SFC_{ME} = 175 g/kWh.

Specific fuel consumption of the auxiliary engine, SFC_{AE} = 200 g/kWh.

Waiting time, t_{wait} = 3 days. Low-speed transit duration, t_{low} = 12 h.

Fuel-based emission factors: 3.114 g/g for CO_2; 1.0×10^{-2} g/g (10 g/kg fuel) for SO_2; 1.5×10^{-2} g/g (15 g/kg fuel) for NO_x; and 2.0×10^{-3} g/g (2 g/kg fuel) for $PM_{2.5}$.

Appendix A.2. Step-by-Step Calculation

Step 1. Conversion of the waiting time to hours. t_{wait} = 3 days × 24 h/day = 72 h.

Step 2. Energy delivered by the auxiliary engines at anchorage. $E_{AE} = P_{AE} \times LF_{AE,hotel} \times t_{wait}$ = 1500 kW × 1.00 × 72 h = 108,000 kWh.

Step 3. Fuel consumed at anchorage (Equation (2)). $m_{wait} = E_{AE} \times SFC_{AE}$ = 108,000 kWh × 200 g/kWh = 21,600,000 g, hence FC_{wait} = 21,600,000 g ÷ 10^6 = 21.60 t.

Step 4. Main engine power under the controlled transit regime. $P_{ME,low} = P_{ME,rated} \times LF_{ME,low}$ = 24,000 kW × 0.20 = 4800 kW.

Step 5. Energy delivered by the main engine at low speed. $E_{ME} = P_{ME,low} \times t_{low}$ = 4800 kW × 12 h = 57,600 kWh.

Step 6. Fuel consumed at low speed (Equation (3)). $m_{low} = E_{ME} \times SFC_{ME}$ = 57,600 kWh × 175 g/kWh = 10,080,000 g, hence FC_{low} = 10,080,000 g ÷ 10^6 = 10.08 t.

Step 7. Total additional fuel consumption. $FC_{add} = FC_{wait} + FC_{low}$ = 21.60 t + 10.08 t = 31.68 t.

Step 8. Pollutant masses (Equation (4)). CO_2: 31.68 t × 3.114 g/g = 98.65 t. SO_x: 31.68 t × 1.0 × 10^{-2} g/g = 0.3168 t (316.8 kg). NO_x: 31.68 t × 1.5 × 10^{-2} g/g = 0.4752 t (475.2 kg). $PM_{2.5}$: 31.68 t × 2.0 × 10^{-3} g/g = 0.0634 t (63.4 kg).

Appendix A.3. Consistency Check Against Equation (1)

The same result is obtained directly from Equation (1) by summing up the two engine components (ME and AE) and the two operational modes (hoteling and controlled transit):

$$E_{CO2} = [(1500 \times 1.00 \times 72 \times 200 \times 3.114) + (24{,}000 \times 0.20 \times 12 \times 175 \times 3.114)] \times 10^{-6} = (67{,}262{,}400 + 31{,}389{,}120)\ \text{g} \times 10^{-6} = 98.65\ \text{t}\ CO_2.$$

The agreement between Equations (1) and (2)–(4) confirms that the mode-specific formulations of Equations (2) and (3) are algebraically identical to the general bottom-up formulation of Equation (1) once the power terms are load-adjusted.

Appendix A.4. Unit Conversions Applied

Mass: 1 t = 10^3 kg = 10^6 g.

Specific fuel consumption: 1 kg/kWh = 10^3 g/kWh.

Emission factors (mass ratios): 1 g/kg = 10^{-3} g/g, and 1 t pollutant/t fuel = 1 g pollutant/g fuel.

Time: 1 day = 24 h.

References

1. UNCTAD. *Strait of Hormuz Disruptions Implications for Global Trade and Development (UNCTAD/OSG/TT/INF/2026/1)*; United Nations Conference on Trade and Development: Geneva, Switzerland, 2026.
2. CFR. *Conflict-Driven Chokepoint Disruptions Crisis Response Playbook No. 4*; Council on Foreign Relations: New York, NY, USA, 2026.
3. Tamburri, M.N.; Carlton, J.T.; Blakeslee, A.M.H.; Bortolus, A.; Canning-Clode, J.; Carvalho, S.; Chang, A.L.; Davidson, I.C.; Donelan, S.C.; Drake, L.A.; et al. Closure of the Strait of Hormuz May Trigger a Bioinvasion Super-Spreader Event. *Biol. Invasions* **2026**, *28*, 177. [CrossRef]
4. UNCTAD. *Vulnerability of Supply Chains Exposed as Global Maritime Chokepoints Come Under Pressure*; United Nations Conference on Trade and Development: Geneva, Switzerland, 2024.
5. MarineTraffic Persian Gulf Vessel Density and Anchorage Analytics. MarineTraffic Intelligence Platform 2026. Available online: https://www.marinetraffic.com/en/ais/home/centerx:63.5/centery:25.0/zoom:6 (accessed on 21 July 2026).
6. Lee, Y.; Park, Y.; Kim, G.; Yoo, J.; Pinzon-Acosta, C.; Gonzalez-Olivardia, F.; Cruz, E.; Lee, H. Ship Air Emission and Their Air Quality Impacts in the Panama Canal Area: An Integrated AIS-Based Estimation During Hotelling Mode in Anchorage Zone. *J. Mar. Sci. Eng.* **2025**, *13*, 1888. [CrossRef]
7. Fuentes, G.; Adland, R. Greenhouse Gas Mitigation at Maritime Chokepoints: The Case of the Panama Canal. *Transp. Res. D Transp. Environ.* **2023**, *118*, 103694. [CrossRef]
8. IMO. *Fourth IMO GHG Study 2020*; International Maritime Organization: London, UK, 2021.
9. Mersin, K.; Alkan, G.; Mısırlıoğlu, T. A New Method for Calculating Fuel Consumption and Displacement of a Ship in Maritime Transport. *Cogent Eng.* **2017**, *4*, 1415107. [CrossRef]

10. Notteboom, T.; Haralambides, H.; Cullinane, K. The Red Sea Crisis: Ramifications for Vessel Operations, Shipping Networks, and Maritime Supply Chains. *Marit. Econ. Logist.* **2024**, *26*, 1–20. [CrossRef]
11. IEA. *Strait of Hormuz Factsheet*; The International Energy Agency: Paris, France, 2026.
12. Shepard, J.U.; Pratson, L.F. Maritime Piracy in the Strait of Hormuz and Implications of Energy Export Security. *Energy Policy* **2020**, *140*, 111379. [CrossRef]
13. Gao, T.; Lu, J. The Impacts of Strait and Canal Blockages on the Transportation Costs of the Chinese Fleet in the Shipping Network. *Marit. Policy Manag.* **2019**, *46*, 669–686. [CrossRef]
14. Huang, D.; Wang, S.; Loughney, S.; Wang, J. Evolutionary Game Model of Strategic Maritime Transport Passages: A Case of the Strait of Hormuz. *J. Mar. Sci. Eng.* **2022**, *10*, 346. [CrossRef]
15. Lyu, D.; Zhao, P.; Zhu, W.; Li, W.; Ling, Y.; Pang, L.; Zhang, S.; Xu, Y. Impact of Russia–Ukraine Conflict on Global Crude Oil Shipping Carbon Emissions. *J. Transp. Geogr.* **2025**, *128*, 104311. [CrossRef]
16. Xiao, R.; Xiao, T.; Zhao, P.; Zhang, M.; Ma, T.; Qiu, S. Structure and Resilience Changes of Global Liquefied Natural Gas Shipping Network during the Russia–Ukraine Conflict. *Ocean Coast. Manag.* **2024**, *252*, 107102. [CrossRef]
17. Gao, G.; Zhao, Y.; Fang, Z.; Xu, L.; Wang, Q. Construction of Global Maritime LPG Trade Multi-Layer Network Models and Pattern Analysis. *Energy Rep.* **2026**, *15*, 108990. [CrossRef]
18. Yi, W.; Wang, X.; He, T.; Liu, H.; Luo, Z.; Lv, Z.; He, K. The High-Resolution Global Shipping Emission Inventory by the Shipping Emission Model (SEIM). *Earth Syst. Sci. Data* **2025**, *17*, 277–292. [CrossRef]
19. Meza, A.; Ari, I.; Al Sada, M.; Koç, M. Disruption of Maritime Trade Chokepoints and the Global LNG Trade: An Agent-Based Modeling Approach. *Marit. Transp. Res.* **2022**, *3*, 100071. [CrossRef]
20. Luo, X.; Yan, R.; Wang, S. After Five Years' Application of the European Union Monitoring, Reporting, and Verification (MRV) Mechanism: Review and Prospectives. *J. Clean. Prod.* **2024**, *434*, 140006. [CrossRef]
21. Wang, S.; Jia, H.; Lu, J.; Yang, D. Crude Oil Transportation Route Choices: A Connectivity Reliability-Based Approach. *Reliab. Eng. Syst. Saf.* **2023**, *235*, 109254. [CrossRef]
22. Wang, X.; Du, D.; Peng, Y. Assessing the Importance of the Marine Chokepoint: Evidence from Tracking the Global Marine Traffic. *Sustainability* **2023**, *16*, 384. [CrossRef]
23. EMSA/THETIS-MRV. Public GHG Emission Reports. European Commission, European Maritime Safety Agency 2026. Available online: https://mrv.emsa.europa.eu/#public/emission-report (accessed on 10 July 2026).
24. Global Maritime Traffic. AIS Vessel Tracking and Density Data Analytics 2026. Available online: https://globalmaritimetraffic.org/gmtds.html (accessed on 9 July 2026).
25. *ISO/IEC Guide 98-3:2008*; Uncertainty of Measurement—Part 3: Guide to the Expression of Uncertainty in Measurement (GUM:1995). International Organization for Standardization: Vernier, Switzerland; International Electrotechnical Commission: Vernier, Switzerland, 2008.
26. IMO; MEPC. *Index of MEPC Resolutions and Guidelines Related to MARPOL Annex VI*; International Maritime Organization: London, UK, 2009.
27. UNFCCC. Adoption of the Paris Agreement. In *United Nations Framework Convention on Climate Change FCCC/CP/2015/L.9/Rev.1*; United Nations Framework Convention on Climate Change: Paris, France, 2015.
28. Britannica. *Strait of Hormuz*; Encyclopedia Britannica Inc.: Chicago, IL, USA, 2026.
29. EIA. *World Oil Transit Chokepoints*; U.S. Department of Energy, Energy Information Administration: Washington, DC, USA, 2024.
30. IMO; MEPC. *63/23/10 2012 Guidelines on Survey and Certification of the Energy Efficiency Design Index (EEDI)*; International Maritime Organization: London, UK, 2012; Volume Annex 10.
31. EEA. *EMEP/EEA Air Pollutant Emission Inventory Guidebook 2023: Technical Guidance to Prepare National Emission Inventories EEA Report No. 07/2023*; European Environment Agency: Copenhagen, Denmark, 2023.
32. Wärtsilä. *Wärtsilä 31 Engine Project Guide: Specific Fuel Oil Consumption (SFOC) Specifications*; Wärtsilä Corporation: Helsinki, Finland, 2021.
33. Everllence. *CEAS Engine Calculation and SFOC Technical Data Sheets*; Everllence SE: Augsburg, Germany, 2026.
34. *ISO 8178-4:2020*; Reciprocating Internal Combustion Engines—Exhaust Emission Measurement—Part 4: Steady-State and Transient Test Cycles for Different Engine Applications. International Organization for Standardization: Vernier, Switzerland, 2020.
35. IMO. *2022 Guidelines for the Development of a Ship Energy Efficiency Management Plan (SEEMP) (Resolution MEPC.346(78)*; International Maritime Organization: London, UK, 2022.
36. OCIMF. *International Safety Guide for Oil Tankers and Terminals (ISGOTT)*, 6th ed.; Oil Companies International Marine Forum: London, UK; International Chamber of Shipping: London, UK, 2020.

37. IMO. *IMO Strategy on Reduction of GHG Emissions from Ships Annex 15, Resolution Mepc.377(80)*; International Maritime Organization: London, UK, 2023.
38. UNCTAD. *Suez and Panama Canal Disruptions Threaten Global Trade and Development*; United Nations Conference on Trade and Development: Geneva, Switzerland, 2024.

Disclaimer/Publisher's Note: The statements, opinions and data contained in all publications are solely those of the individual author(s) and contributor(s) and not of MDPI and/or the editor(s). MDPI and/or the editor(s) disclaim responsibility for any injury to people or property resulting from any ideas, methods, instructions or products referred to in the content.